Heliyon 10 (2024) e25511

Contents lists available at ScienceDirect

Heliyon

journal homepage: www.cell.com/heliyon

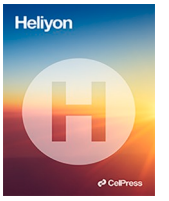

Research article

Structural, magnetic, electric and electrochemical studies on zinc doped magnesium ferrite nano particles - Sol-gel method

T. Senthamilselvan [a,1], S. Nithiyanantham [a,*,1], K. Kogulakrishnan [a,1], S. Mahalakshmi [b], T. Lakshmigandhan [a,1], R. Mohan [c], B. Gunasekaran [d]

[a] Department of Physics, Thiru.Vi.Ka Government Arts College Thiruvarur, Tamilnadu- 610003, India
[b] Department of Physics, Ethiraj College for women Chennai, Tamilnadu -600008, India
[c] Department of Chemistry, AMET University, Kanathur, Chennai - 603112, India
[d] Department of Physics, SRM University, Kattankulathur, Chennai, 603203, India

ARTICLE INFO

Kerywords:
Ferrites
Structural
Magnetic
Dielectric
Electrochemical

ABSTRACT

The sol-gel process was used to prepare zinc doped magnesium ferrite ($Mg_{1-x}Zn_xFe_2O_4$) nano-powders obtained from the nitrates of magnesium, zinc and ferrous is precursor materials, maintain the pH value which were then studied for sensing purposes. The crystallite size and phase of the ferrite samples studied by X-ray diffraction (XRD) revealed a pure spinel phase ($Mg_{1-x}Zn_xFe_2O_4$) with a cubic spinel structure and higher crystallite size and etc. The functional groups with possible stretching analysis were taken from Fourier transform infrared spectroscopy (FTIR). The surface features and morphology and the purity of the samples were analysed through a Scanning electron microscope (SEM) and energy dispersive X-ray (EDAX) spectrum respectively. Through the vibrating sample magnetometer (VSM), the magnetic behaviour was studied from relevant parameters such as saturation magnetization (Ms), coercivity (Hc) and retentivity (Mr). The larger Ms in 0.8 has ferromagnetic nature were observed. The dielectric constants (ε'& ε''), dielectric loss (tan δ) with AC conductivity (σ_{AC}) determined through the LCR metre, and electrochemical behaviour of the samples were found through cyclic voltametery. The possible polarizations at lower and higher frequencies are studied The obtained data are extensively examined and understood.

1. Introduction

In recent times, the needs of magnetic ferrites in nano phase are increased due to a technological development. Nano ferrites serve a significant role in technical applications and are often used in high-frequency electronics. Ferrites excel in high frequency applications because to their high resistivity, low magnetic, and dielectric losses [1]. They are sometimes referred to as multiferroics due to their dielectric behaviour. They are commercially important because they can be utilized in a wide range of products, including phase shifters, high frequency transformer cores, televisions and many electronic goods [2–4]. The dielectric characteristics of ferrites are affected by various parameters, including manufacturing method, composition, and particle size [5,6]. Due to their high electrical resistivity, low magnetic loss, and low dielectric losses, $MgFe_2O_4$ and similar ferrites are frequently utilized as components in the

* Corresponding author.
E-mail addresses: s_nithu59@rediffmail.com, prof.s.nithiyanantham@tvkgac.co.in (S. Nithiyanantham).
[1] Bharathidasan University, Thiruchirapalli.

https://doi.org/10.1016/j.heliyon.2024.e25511
Received 18 November 2023; Received in revised form 22 January 2024; Accepted 29 January 2024
Available online 1 February 2024

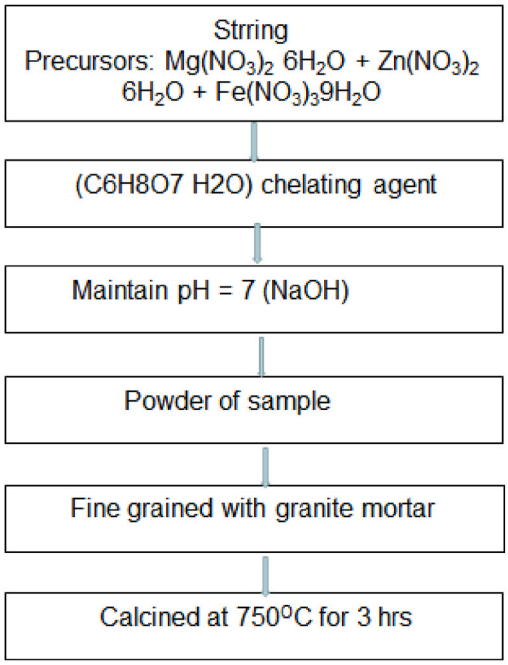

Fig. 1. Experimental flow chart.

microwave family [7], we examined their dielectric behaviour at ambient temperature over a wide frequency range. In some cases, generated nano-sized $MgCrxFe_2xO_4$ compounds with varying quantities of Cr under the idea that substituting Fe^{3+} ions for Cr^{3+} ions will increase dielectric characteristics. Magnesium Ferrites substituted with Cr^{3+} ions at the B site should improve electrical resistance. The goal of Cr^{3+} ion replacement for Fe^{3+} ions in this work is to reduce dielectric loss. Materials which possess magnetic and dielectric owning to many devices Phase Shifter, high frequency transformer cores, switches, resonators, computers, TVs, mobile phones and many. Because MgFe2O4 and similar ferrites have low magnetic and dielectric losses and high electrical resistivity, they are frequently employed as components in the microwave family [8].

It is mostly employed for magnetostrictive applications, such as sensors and actuators, due to its high saturation magnetostriction (200 ppm) [9]. $MgFe_2O_4$ is a good alternative to Terfenol-D because it doesn't include any rare earth elements [10]. Furthermore, its magnetostrictive characteristics can be modified by creating magnetic uniaxial anisotropy [11]. This can be done by magnetic annealing [12], magnetic field assisted compaction [13], or reaction under uniaxial pressure, [14]. This final solution has the benefit of being extremely quick (20 min) due to the usage of spark plasma sintering. The cobalt ferrite's produced magnetic anisotropy further enhances the magnetoelectric effect in composites [15]. The micro/nano structured materials possess some tremendous mechanical behaviour such as size dependent elasticity, tensile strength, residual stress, eigenstrain, young's modulus and etc., [16,17].

Metallic materials with a nano-crystalline structure and non-classical features were modified as a result of the creation of new magnetic systems, such as iron based magnetic systems. Numerous advances in science and technology have resulted from the production process development in the size control and characterisation of these magnetic systems. The manufacture of nano-ferrite nanoparticles using chemical methods has attracted a lot of interest in the search for better materials with adjustable shape, nanoscale, and stability for a variety of applications. Sol-gel techniques [18]. The method of synthesizing the nanoparticle required some key parameter to enhancing the efficiency is homogeneity, uniform distribution of dopants at the molecular and atomic level. Further, structural, electrical and magnetic properties enehanced through the proper addition of dopant can be added easily in sol-gel process working at low temperature. The dielectric constant and its related parameters are mostly required in all fields of science, engineering and technology. Since the value of dielectrics, materials with more dielectric constant requires for mass storage devices, while the lower value of dielectric constant materials can be able to active in millimetre region and so useful in wireless communication mainly for fast signalling process [19].

Ferrites that are quite tough on the other hand, permanent ferrite magnets are made of hard ferrites that have great coercivity and remanence after magnetization. Iron oxide and barium or strontium carbonate are used to make hard ferrite magnets [20,21]. The materials are extremely resistant to demagnetization because of their high coercivity, which is a need for a permanent magnet. Additionally, they have a high magnetic permeability. Materials with more anisotropic constant needed for some medical and sensing applications [22], the properties with magneto-optic, recording media, microwave devices, wireless devices, and injection-molded pieces [23]. Ceramic magnets are widely used in household products, such as refrigerator magnets, and are reasonably priced. The magnetic field strength H varies between 30 and 160 kA turns per metre (400–2000 Oe), and the maximum magnetic field B is roughly 0.35 T [24]. The density of ferrite magnets is approximately 5 g/cm3.

Among this various synthesis process here, the authors used the sol-gel method of synthesis has many advantages such as simple to

Table 1
Lattice and other related parameters of synthesised samples.

Conc.	Lattice constant (a) A°	Planar distance (d) A°	Particle size (D) nm	Lattice strain (ε)	Dislocation density (δ)	X-ray density (ρ)	Hoping length site A (L_A) A°	Hoping length site B (L_B) A°
0.0	8.347	2.055	21.06	16.12	4.37	8.34	3.61	2.95
0.2	8.295	2.042	39.42	3.45	1.09	4.51	3.59	2.93
0.4	8.275	2.038	23.23	4.61	2.21	5.79	3.58	2.92
0.6	8.297	2.043	44.37	2.30	6.79	5.74	3.59	2.93
0.8	8.305	2.044	18.41	14.94	5.03	8.19	3.59	2.93

operate, time consuming, costless and etc., and efficient process than the other synthesis methods [25,26]. We used the sol-gel method to create $Mg_{1-x}Zn_xFe_2O_4$ (x = 0, 0.2, 0.4, 0.6, 0.8) soft ferrite samples in this study. The samples' structural, morphological, magnetic and dielectric properties have all been examined.

2. Sample preparation

Sol-gel powders of zinc substituted magnesium ferrite $Mg_{1-x}Zn_xFe_2O_4$ (x = 0, 0.2, 0.4, 0.6, 0.8) were produced. As raw materials, the analytical grades $Mg(NO_3)_2$ $6H_2O$, $Zn(NO_3)_2$ $6H_2O$, $Fe(NO_3)_3 9H_2O$, citric acid ($C_6H_8O_7$ H_2O), and sodium hydroxide (NaOH) were employed. For all samples, a stoichiometric amount of Mg, Zn, Fe, metal salts were dissolved in 100 ml double distilled water in the proper molar ratio (MgZn:Fe in 1:2). The solutions have been mixed and agitated until they are clear. Metal nitrates were used in a 1:1 mol ratio with citric acid. To keep the pH at 7, a solution of metal nitrates was added drop by drop to a solution of 1 M sodium hydroxide to produce nanoparticles that are chemically homogeneous and less scattered in size [27]. The dry (MZFO) powder was obtained from the previously described sol-gel technique maintain the temperature of heated hot plate at 90 °C. The precipitates were crushed into powder using a granite mortar and pestle, and the dried powder was calcined at 750 °C for 3 h to generate well-crystalline nanoparticles using heat furnace and they allow attaining the room temperature. The sol-gel process is depicted in Fig. 1.

3. Materials characterization

The XRD patterns were captured at room temperature using an X-ray diffractometer (λ = 1.5406 A°) (RIGOKU, MINIFLEX-JAPAN). An FT-IR analysis helps examining the formation and dissolution of functional groups on KBr pellets containing 1 % (w/w) material (ALPHA-TFT-Spectrometer). The surface features and the morphological analysis carried out through SEM analysis (Scanning electron microscope FEI Company Netherlands). The magnetic field was measured by a vibrating-sample magnetometer. The magnetic behaviour tested through vibrating sample magnetometer (VSM-LAKESHORE-USA). The dielectric measurements performed with LCR HI-Tester (HIOKI 3532-50) of frequency up to 5 MHz. The cyclic voltmeter used for the electrochemical analysis (VERSA STAT MC –Princeton Applied Research).

4. Results and discussion

4.1. XRD patterns analysis

From the X-ray spectra of magnesium ferrite with different concentrations of Zn dopants. The respective peaks and their hkl values are indexed and their values are compared with the similar reports [28–30].The major peaks with their respective hkl values are (220), (311), (401), (422), (511) observed. The single phase cubic spinel structure was indicated from the above peaks. The prominent peak at (311) are used to calculate the crystalline size through Debye Scheror formula as equation (1),

$$D = \frac{K\lambda}{\beta \cos\theta} \tag{1}$$

Further the lattice strain (ε), dislocation density (δ) and x-ray density (D_x) are computed from the following equations (2)–(4)

$$\varepsilon = \beta \cos\theta / 4 \tag{2}$$

$$\delta = 1/D^2 \tag{3}$$

$$D_x = \frac{8M}{Na^3} \tag{4}$$

Where, M − is the molecular weight, and N- Avagadro's number.

The hoping length in site A and B are respectively L_A and L_B [20,31,32], were determined through the following relations (5) and (6),

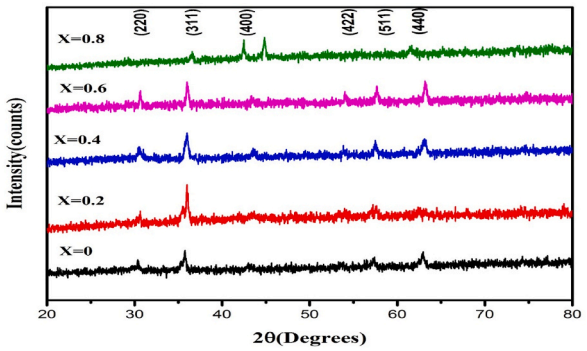

Fig. 2. XRD spectra of $Mg_{1-x}Zn_xFe_2O_4$ ($x = 0, 0.2, 0.4, 0.6, 0.8$).

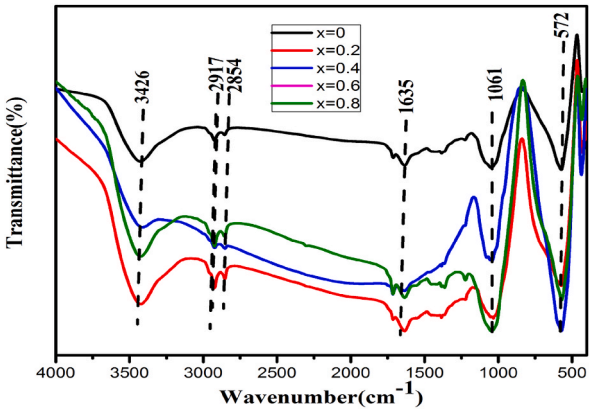

Fig. 3. Ftir spectra of $Mg_{1-x}Zn_xFe_2O_4$ ($x = 0, 0.2, 0.4, 0.6, 0.8$).

$$L_A = \frac{a \times \sqrt{3}}{4} \tag{5}$$

$$L_B = \frac{a \times \sqrt{3}}{2} \tag{6}$$

The lattice parameters and other parameters are presented in Table .1.

In general half of Fe^{3+} ions with Zn^{2+} ions in octahedral position and the remaining Fe^{3+} ions are exist in tetrahedral site. The increase in lattice parameter may arise due to the substitution of Fe^{3+} iron by other ions in tetrahedral sites. The decrease and increase in crystallite size suggesting the unfavoured and favour of crystallization relative to long ionic radii.

Fig. 2 depicts the XRD patterns for all five compounds, scanned from 20° to 90°. The XRD pattern's fluctuating intensity of the direction line confirms the polycrystalline nature of the synthesised ferrite. The direction patterns' maximum intensity peaks, at roughly 35.2, correlate to the main phase of MgZn ferrite nanoparticle. Peaks attributed to reflection planes (220), (311), (400), (422), (511), (440), and (335) correspond well with MgZn ferrite standard direction peaks (JCPDS (10–0467)) and are marked as (cubic spinal phase). The particle size had a similar effect on the lattice constant of MgZn ferrite. There are different lattice constant values for increasing the dopant of Zn^{2+} ions, as seen in Table 1. The variation in lattice parameter is most likely the result of smaller Mg^{2+} ions (0.72 A) being replaced by larger Zn^{2+} ions (0.74 A) [33,34]. Scherrer's formula [35,36] estimates the average crystallite size of the examined samples to be around (18–44) nm for varied compositions. The small reduction in crystallite size caused by the addition of Zn demonstrates that the presence of zinc impedes crystal formation [37,38]. The observed crystallite size fluctuation in Zn^{2+} substituted Mg ferrite confirms the variation in lattice constant. From 0.0 to 0.4 the lattice constant gets decreased due to John- Tellar distortion, while 0.6 and 0.8 it get increased on the basis of Vegard's law.

4.2. FT-IR spectral analysis

The chemical compositions with related analysis were determined through the FT-IR spectrum of produced $Mg_{1-x}Zn_xFe_2O_4$ ferrite nano-composites (x at varied concentrations (X = 0.0, 0.2, 0.4, 0.6, and 0.8) of synthesised samples. Figure (3) depicts the FT-IR spectrum of $Mg_{1-x}Zn_xFe_2O_4$ ferrite. Analyses of 567–667, 1640, and 3420 cm^{-1} reveal numerous different peaks. And each samples

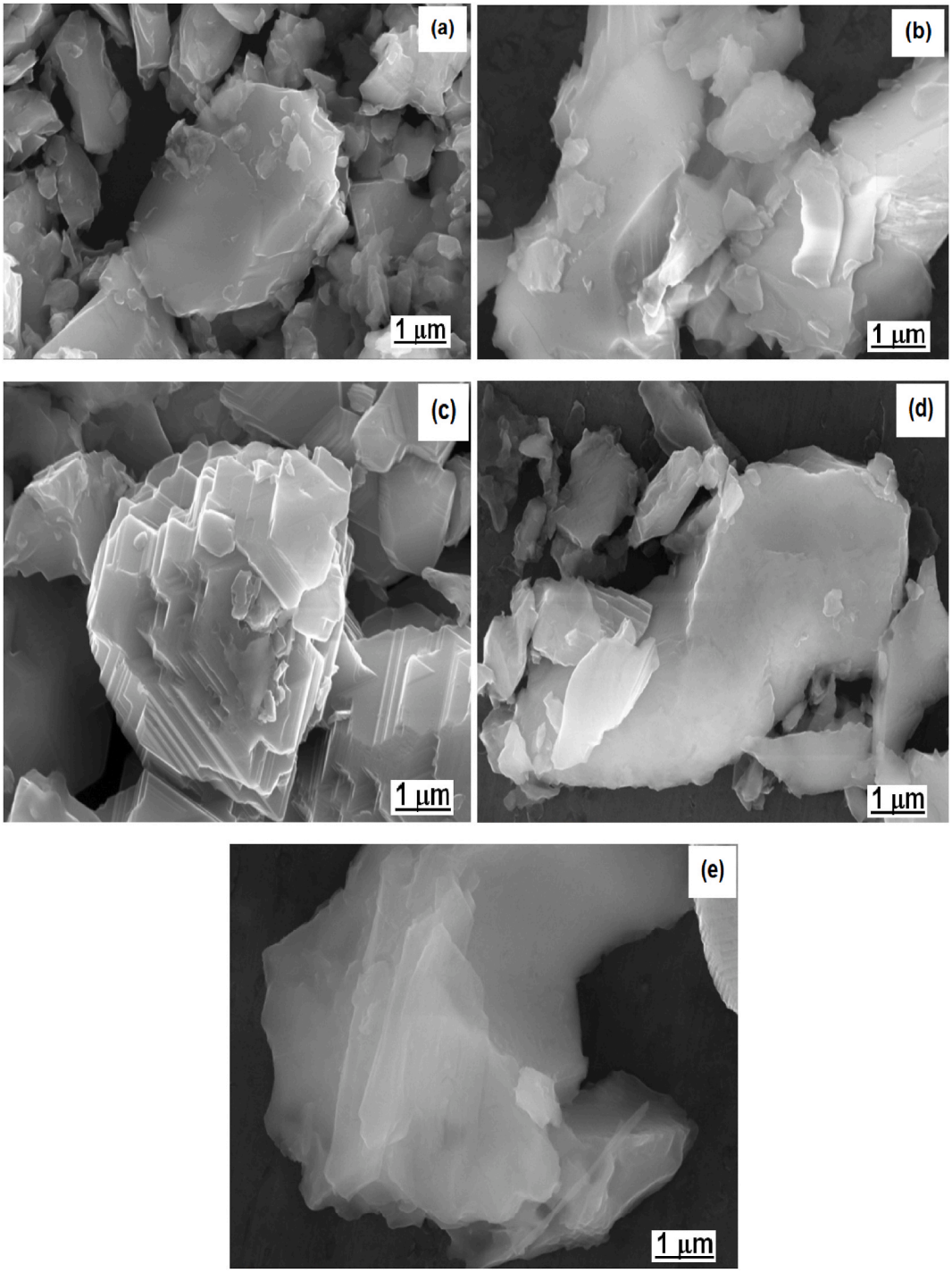

Fig. 4. (a–e). SEM images of $Mg_{1-x}Zn_xFe_2O_4$ (x = 0, 0.2, 0.4, 0.6, 0.8).

showed characteristics peaks of O–H stretching and H–*O*–H bending vibrations situated at 3420 and 1640 cm^{-1}, respectively.The vibrations of Mg–O, Fe–O, and Zn–O bonds at octahedral and tetrahedral sites were occurred at lower frequency regions. The FTIR results from ferrite systems, which have a broad spectrum at 400-600 cm^{-1}, correspond well with these findings [38–42]. Furthermore, the C═C bending vibrations was observed at 2338 and 2934 cm^{-1} [43].

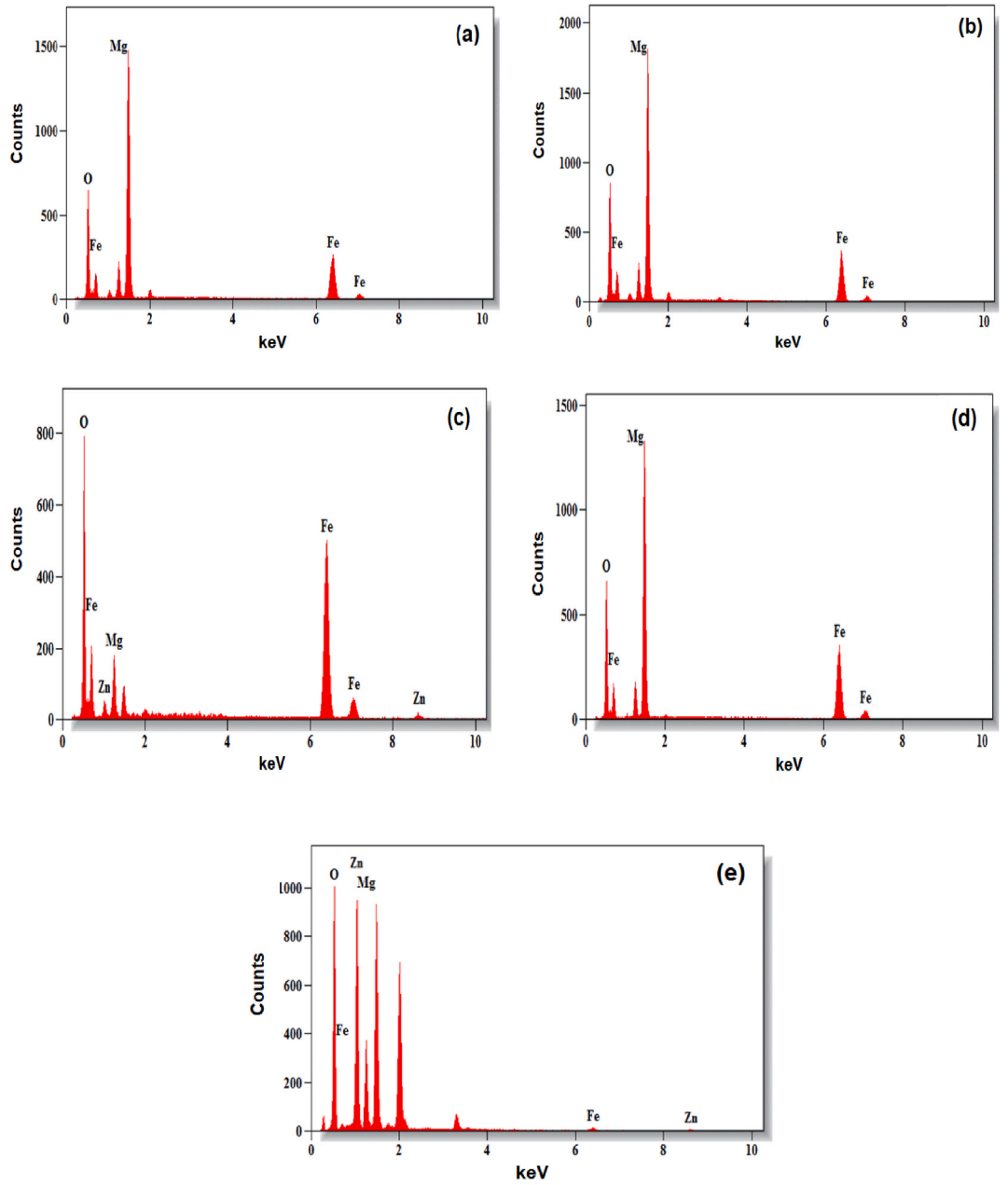

Fig. 5. (a–e). EDAX spectra of $Mg_{1-x}Zn_xFe_2O_4$ ($x = 0$, 0.2, 0.4, 0.6, 0.8).

4.3. SEM and EDAX analysis

The SEM images for Zn-doped $MgFe_2O_4$ in a 1 μm ranges are shown in Fig. 4(a–e). The micrographs clearly show the clear morphology and defined features. At 0.2 and 0.4, the image gets better, and at 0.6, an aggregation phenomenon-induced smooth, clear image is fine compared to other concentrations. Additionally, the XRD results show that the average particle size is approaching. But, some intriguing natures of images are necessary to discuss. For 4(a) some smaller size particle appeared. In 4(b) the changes are appeared relatively more compare to 4 (a). But, in 4 (c & d) the particle sizes changes considerably from smaller to elongated layer structure has become more numerous. And in 4(e) the layered structure are very larger. These results were reflects through changes in intensity and wider peak in XRD spectra [44]. Fig. 5(a–f) displays the EDAX analysis and it shown the composition and purity. Furthermore, it is evident that the sample is free of any impurities.

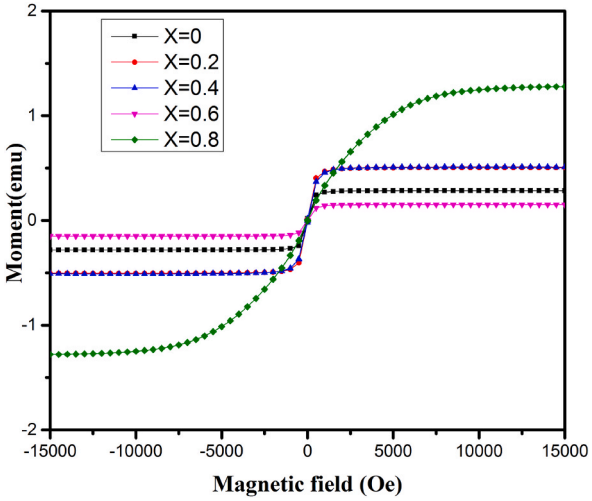

Fig. 6. VSM spectra of $Mg_{1-x}Zn_xFe_2O_4$ ($x = 0$, 0.2, 0.4, 0.6, 0.8).

Table 2
Magnetic parameters.

Sample code (X)	Coercivity (H_c) (Oe)	Saturation magnetization (M_s) (emu/g)	Retentivity (M_r) (10^{-3} emu/g)
0.0	35.275	0.28440	18.286
0.2	15.243	0.50558	12.680
0.4	24.593	0.51192	18.971
0.6	9.3016	0.15132	2.2376
0.8	14.480	1.27910	5.6662

4.4. VSM analysis

The magnetic characteristics of the produced samples were subjected to magnetic analysis using VSM (15 kOe). Fig. 6 depicts the resulting magnetic hysteresis. This hysteresis loop was used to investigate the relationship between respective magnetic characteristics measurements. Table 2 shows the Ms and Hc values for various Mg–Zn concentrations. The saturation magnetization decreased significantly as the concentration climbed from 0.0 to 0.8 due to a decrease in the phase content of $MgZnFe_2O_4$ (Table 1). Fig. 5 also shows that the saturation magnetization (Ms) value for the $MgZnFe_2O_4$ sample is greater in 0.8 (1.28 emu/g) than in other concentrations. This could be attributed to the great crystallinity and homogeneous morphologies shown in Fig. 3. The Ms values dropped dramatically at concentration 0.6, it can be explained by $MgZnFe_2O_4$ phase (Table 2). The hysteresis curves of MgZn Ferrite calcined at 0.8 reveal ferromagnetic behaviour, however at 0.4 it behaved as a weak ferromagnetic and at 0.6 as an antiferromagnetic [45,46]. The replacement of non-magnetic Zn^{2+} ions with magnetic Mg^{3+} ions changes the behaviour in site B. The effect of replacement of Zn^{2+} over the Ms, Mr and Hc values increasing with the concentration of Zn^{2+}, whereas the decrement in those respective parameters due to canting effect [47].

This is due to the sample's reduction of the MgZn Ferrite phase and the emergence of antiferromagnetic Fe_2O_3 phases. A coercive field exists when M and H change sign, and there is a small amount of coercivity was observed, which was attributed to the characteristic soft ferromagnetic behaviour of MgZn Ferrite and the particles in nano-phase found from X-ray analysis. The coercivity of $MgZnFe_2O_4$ increased with increasing concentration, which could be attributed to irregular big holes on grain borders obstructing [34,48,49].

4.5. LCR analysis

The dielectric constant vs. frequency for samples was presented in Fig. 7 (a)-(d). Fig. 7(a) shows that the dielectric constant decreases with increasing frequency suggesting the dispersions phenomena with frequency. The decrease in dielectric constant at lower frequency after reaching 3 it attaining lower further frequency it shown almost constant for all frequencies. The changes in the dielectric constant due to polarization mechanism given by the valence state electrons. While at high frequencies region the causing in response due to the polarization effect and the applied field not influencing polarization. And the occurrence of polarization occur at lower frequencies are referred as interfacial polarization and there is no interfacial are any type of polarization is high frequency region.

The dielectric behaviour can be explained based on the M − W interfacial model which is mostly depends on heterogeneous

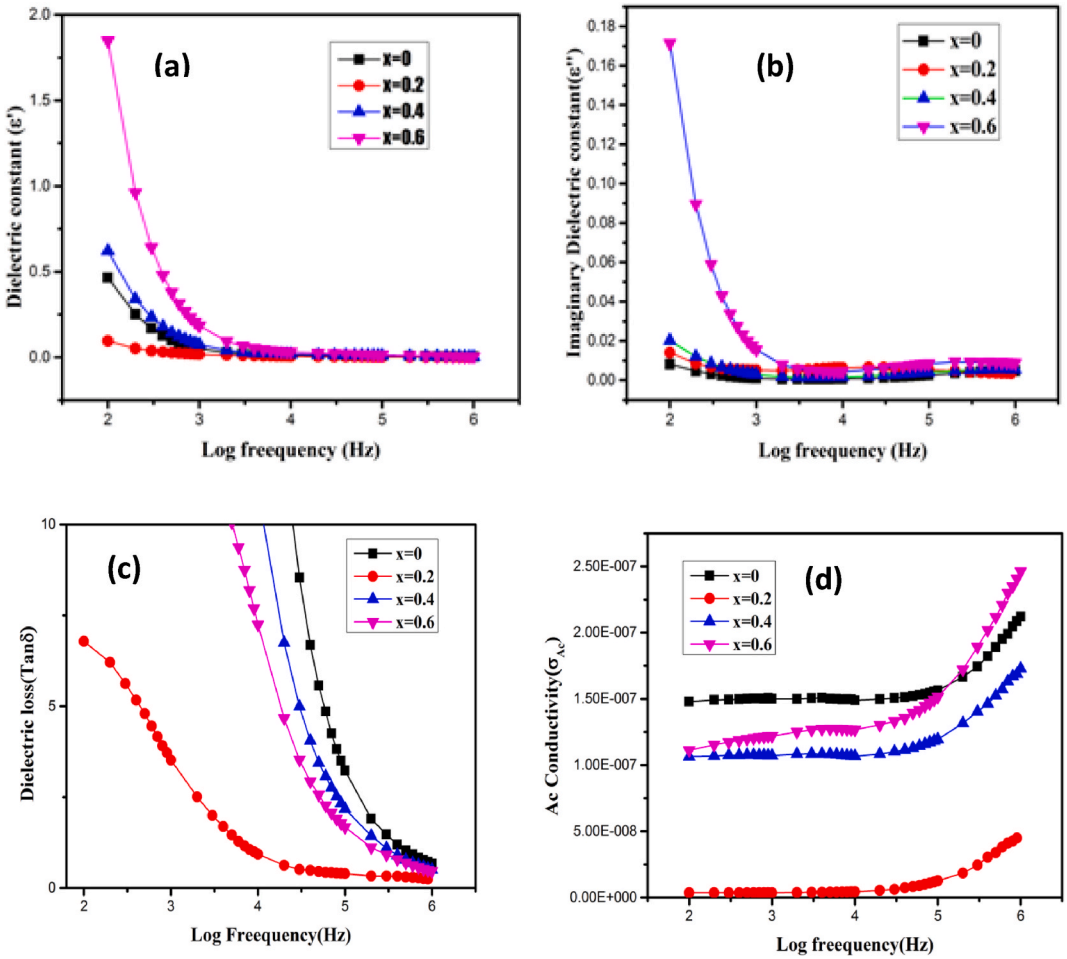

Fig. 7. Log Frequency Vs (a) dielectric constant, (b) imaginary dielectric constant, (c) dielectric loss and (d) AC conductivity of $Mg_{1-x}Zn_xFe_2O_4$ (x = 0, 0.2, 0.4, 0.6, 0.8).

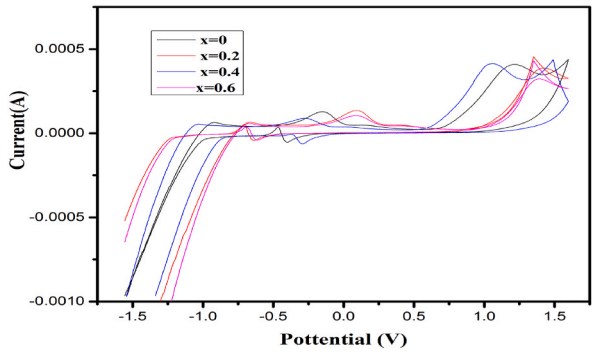

Fig. 8. V - I characteristics of $Mg_{1-x}Zn_xFe_2O_4$ (x = 0, 0.2, 0.4, 0.6, 0.8).

structure pushing grain and grain boundary. Initially at lower frequencies the valence state electrons responses to electric field and reaches the grain boundary and accumulated and its leads to interfacial polarization under applied electric field. There is a decrease and constant values for polarization in higher frequencies due to the magnetic moment not synchronized in the applied electric field. The dielectric constant becomes frequency independent at higher frequencies. It results from electric dipoles' incapacity to track the applied electric field's rapid fluctuation. Further, The exchange in electron between Fe^{3+} and Fe^{2+} lagging behind the applied frequency. It reveals that nearly constant dielectric constant at higher frequency. While larger dielectric constant at lower frequency

causes due to heterogeneous effect, pores, grain surfaces and layers.

Fig. 7(b) depicts the change in dielectric loss vs. frequency. It shows the same trend like dielectric constant. It means that at lower frequencies higher loss and at higher frequency it reaches close to zero is the evident that large polarization occurs at lower region rather than higher region. It is the essential parameter to decide the electron behaviour in ferrites. The dielectric loss tangent and with functions of frequencies are depicted in Fig. 7(c). There is a similar and same trend observed for dielectric loss. At lower concentration of the losses are more while increasing the concentration it enhancing the polarization mechanism leads to lower loss tangent values for higher concentration of dopant at lower frequencies. The key parameter related to dielectric constant which gives information about the conductive nature of specimens is shown in Fig. 7(d). It shows the reverse trend as that of loss tangent, ie., at lower frequencies lower conduction due to polarization mechanism and at higher frequencies the increasing conduction leads to lower polarization effect and all the applied field are involving conduction phenomenon leads larger values at higher frequencies region [50–53].

4.6. Cyclic voltametric analysis

Utilizing cyclic voltammetry (CV), the electrochemical activity of $MgFe_2O_4$ with Zn dopant was assessed. A three-electrode setup used to measure the electrochemical reactions [39]. Fig. 8 illustrates the results of cyclic voltammetry experiments using 1 M KOH at a constant scan rate (+0.2 to −0.2V). Using cyclic voltammetry to ascertain the electrode reaction's reversibility, the electrode reaction was quantified with a 10 mV/s scan rate and accounting for the difference in the oxidation potential (EO) with reduction potential (ER) [54]. The trend was more reversible the lower the value of EO-ER. Therefore, the observed capacitance was mostly dependent on the redox mechanism as shown by the CV curve, which depicts a quasi-reversible electron transfer process [55]. From the same figure without dopant the current behaviour is less in both positive and negative directions. In presence of dopants the current get increased on both sides. Almost all compositions it recorded maximum current is same and different lower values. In addition the areas covered by all concentrations are almost same. So, the present samples may suitable for electrochemical application and suitable to fabricate the electrochemical sensor and etc.

5. Conclusions

In present investigation, Sol-gel approach was applied to prepare magnetic magnesium zinc ferrites. From the obtained above results, magnetic Mg–Zn ferrites provide the most important and best benefit for magnetic storage. The XRD pattern of Mg–Zn ferrites shows cubic spinel structure with Fd3m phase group and nano particle range. The produced ferrite has a roughly spherical shape, however some distortion may be noticed after doping. For the Mg–Zn-ferrites, the significant FT-IR absorption peaks at 400 and 500 cm^{-1} represented a Fe–O, Mg–O, and Zn–O vibration band, respectively. The well-defined shape in observed in 0.6 and 0.8 concentration. The ferromagnetic behaviour obtained in 0.8 concentration and the particles sizes approached with XRD analysis. The dielectric constant drops as frequency increases, and $x = 0.8$ has the highest dielectric constant. For all samples, as frequency rises, dielectric loss decreases. The increasing dielectric constant and decreasing their losses are favoured mass storage applications. The electrochemical phenomena influence the magnetic and sensing behaviour. The overall conclusion is that magnetic $Mg_{1-x}Zn_xFe_2O_4$ mixed ferrites are opted materials for making devices such as mass storage and sensing applications.

Funding

There is no funding from any agency

Data Availability statement

The data can be made available on proper request from the editor.

CRediT authorship contribution statement

T. Senthamilselvan: Resources, Methodology, Formal analysis. **S. Nithiyanantham:** Writing – original draft, Supervision, Methodology, Conceptualization. **K. Kogulakrishnan:** Software, Investigation, Conceptualization. **S. Mahalakshmi:** Validation, Formal analysis. **T. Lakshmigandhan:** Visualization, Investigation. **R. Mohan:** Resources, Methodology. **B. Gunasekaran:** Validation, Resources.

Declaration of competing interest

The authors declare that they have no known competing financial interests or personal relationships that could have appeared to influence the work reported in this paper.

References

[1] Y. Yamamoto, A. Makino, T. Yamaguchi, I. Sasada, Fine grained ferrite for low profile transformer, IEEE Transactions,on Magnetics 33 (1997) 3742–3744.
[2] M. Sugimoto, The past, present, and future of ferrites, J Amer Cera Soc 82 (2) (1999) 269–280.
[3] K. Kondo, T. Chiba, S. Yamada, Effect of microstructure on magnetic properties of Ni- Zn ferrites, J Magm Mag Mate 254–255 (2003) 541–543.

[4] L.B. Kong, Z.W. Li, G.Q. Lin, Y.B. Gan, Magneto-dielectric properties of Mg–Cu– Co ferrite Ceramics: II. Electrical, dielectric, and magnetic properties, J Amer Cera Soc 90 (7) (2007) 2104–2112.
[5] R.M. Borade, S. B Somvanshi, S.B. Kale, R.P. Pawar, K.M. Jadhav, Spinel zinc ferrite nanoparticles: an active nanocatalyst for microwave irradiated solvent free synthesis of chalcones, Mater. Res. Express 7 (2020) 016116.
[6] Y. Köseoğlu, H.Ü.S.E.Y.İ.N. Kavas, B. Aktaş, Surface effects on magnetic properties of superparamagnetic magnetite nanoparticles, physica status solidi (a) 203 (7) (2006) 1595–1601.
[7] P.B. Kharat, S.B. Somvanshi, J.S.S.S. Kounsalye, S.S. Deshmukh, P.P. Khirade, K. Jadhav, K, Temperature Dependent Viscosity of Cobalt Ferrite/ethylene Glycol Ferrofluids AIP Conference Proceedings, AIP Publishing), 2018 050044.
[8] M. Raghasudha, D. Ravinder, P. Veerasomaiah, Influence of Cr3+ ion on the dielectric properties of nano crystalline Mg-ferrites synthesized by citrate-gel method, Mater Sci Appls 4 (2013) 432–438.
[9] A.G. Olabi, A. Grunwald, Design and application of magnetostrictive materials, Maters Design 29 (2) (2008) 469–483.
[10] R.S. Turtelli, M. Kriegisch, M. Atif, R. Grössinger, Co-ferrite–A material with interesting magnetic properties, IOP Conference Series: Mate Sci Engg 60 (1) (2014) 012020.
[11] J.C. Slonczewski, Origin of magnetic anisotropy in cobalt-substituted magnetite, Phys. Rev. 110 (6) (1958) 1341.
[12] C.C.H. Lo, A.P. Ring, J.E. Snyder, D.C. Jiles, Mprovement of magnetomechanical properties of cobalt ferrite by magnetic annealing, IEEE Transac Magnes 41 (10) (2005) 3676–3678.
[13] J. Wang, X. Gao, C. Yuan, J. Li, X. Bao, Magnetostriction properties of oriented polycrystalline CoFe2O4, J Magnsm Mag Mater 401 (2016) 662–666.
[14] A. Aubert, V. Loyau, F. Mazaleyrat, M. LoBue, Uniaxial anisotropy and enhanced magnetostriction of CoFe2O4 induced by reaction under uniaxial pressure with SPS, J Europ Cera Soc 37 (9) (2017) 3101–3105.
[15] A. Aubert, V. Loyau, F. Mazaleyrat, M. Lobue, Enhancement of the magnetoelectric effect in multiferroic CoFe2O4/PZT bilayer by induced uniaxial magnetic anisotropy, IEEE Trans. Magn. 53 (11) (2017) 1–5.
[16] S. Ali Faghidian, Analytical approach for inverse reconstruction of eigenstrains and residual stresses in autofrettaged spherical pressure vessels, J Press Ves Tech 139 (4) (2017) p041202.
[17] S. Ali Faghidia, K.K. Žur, E. Pan, Stationary variational principle of mixture unified gradient elasticity, Inter J Engg Sci 182 (2023) 103786.
[18] A. M. El Nahrawy, H. Salah El-Deen, A.A. Soliman, W.M.M. Mosa, Crystallographic and magnetic properties of Al3+ co-doped NiZnFe2O4 nano-particles prepared by sol- gel process, Egyp J Chem 62 (3) (2019) 525–532.
[19] A. M. El Nahrawy, A.B.A. Hammad, A.M. Bakr, A.R. Wassel, Adjustment of morphological and dielectric properties of ZnTiO 3 nanocrystalline using Al2O3 nanoparticles, App Phys A 125 (2019) 1–8.
[20] T. Tatarchuk, M. Myslin, I. Mironyuk, M. Bououdina, A.T. Pedziwiatr, R. Gargula, B.F. Bogacz, P. Kurzydto, Synthesis, morphology, crystallite size and adsorption properties of nanostructured Mg–Zn ferrites with enhanced porous structure, J Alloys Compou 819 (2020) 152945.
[21] D.N. Bhoyar, S.B. Somvanshi, P.B. Kharat, A. Pandit, K. Jadhav, Structural, infrared, magnetic and ferroelectric properties of Sr0· 5Ba0· 5Ti1−xFexO3 nanoceramics: modifications via trivalent Fe ion doping, Physica B 581 (2019) 411944.
[22] A.J. Shebha, T. Arun, R.J. Joseyphus, Role of magnetic anisotropy on the heating mechanism of Co-doped Fe3O4 nanoparticles, Physica B: Cond. Mat. 598 (2020) 412429.
[23] B.C. Brightlin, S. Balamurugan, T. Arun, Microstructural and magnetic features of SrFe 12 O19 materials synthesized from different fuels by sol-gel auto-combustion method, J Superconduc Nov Magm 30 (2017) 1427–1437.
[24] A. Sutka, G. Mezinskis, Sol-gel auto-combustion synthesis of spinel-type ferrite nanomaterials, Frontiers Mater. Sci. 6 (2012) 128–141.
[25] A. Manikandan, J. Judith Vijaya, M. Sundararajan, C. Meganathan, L. John Kennedy, M. Bououdina, Optical and magnetic properties of Mg-doped ZnFe2O4 nanoparticles prepared by rapid microwave combustion method, Superlat Microstruc 64 (2013) 118–131.
[26] Y. Ichiyanagi, M. Kubota, S. Moritake, Y. Kanazawa, T. Yamada, T. Uehashi, Magnetic properties of Mg-ferrite nanoparticles, J Magsm Mag Mats 310 (2) (2007) 2378–2380.
[27] A.M. Gismelseed, K.A. Mohammed, H.M. Widatallah, A.D. Al-Rawas, M.E. Elzain, A.A. Yousif, Structure and magnetic properties of the ZnxMg1-xFe2O4 ferrites, J Phys: Confe Ser 217 (1) (2010) 012138.
[28] K.A.M. Khalaf, A.D. Al-Rawas, H.M. Widatallah, K.S. Al-Rashdi, A. Sellai, A.M. Gismelseed, M. Hashim, S.K. Jameel, M.S. Al-Ruqeishi, K.O. Al-Riyami, M. Shongwe, A.H. Al-Rajhi, Influence of Zn2+ ions on the structural and electrical properties of Mg1− xZnxFeCrO4 spinels, J Alloys Compounds 657 (2016) 733–747.
[29] M.H. Alimuddin, S. Kumar, S.E. Shirsath, R.K. Kotnala, J. Shah, R. Kumar, Synthesis and characterizations of Ni2+ substituted cobalt ferrite nanoparticles, Mat Chem Phys 139 (2–3) (2013) 364–374.
[30] H. Mohseni, H. Shokrollahi, I. Sharifi, Kh Gheisari, Magnetic and structural studies of the Mn- doped Mg–Zn ferrite nanoparticles synthesized by the glycine nitrate process, J Magsm Mag Mate 324 (22) (2012) 3741–3747.
[31] M.M. Rashad, M.G. Fayed, T.M. Sami, E.E. El-Shereafy, Structural, microstructure and magnetic properties of superparamagnetic Mnx Mg1− X Fe2O4 powders synthesized by sol–gel auto-combustion method, J Mate Sci: Mate Electron 26 (2015) 1259–1267.
[32] X. Zhang, Y. Li, R. Liu, Y. Rao, Q. Rong Hand, High-magnetization FeCo nanochains with ultrathin interfacial gaps for broadband electromagnetic wave absorption at gigahertz, ACS appl mate inter 8 (2016) 3494–3498.
[33] K. Verma, A. Kumar, D. Varshney, Dielectric relaxation behavior of AxCo1− xFe2O4 (A= Zn, Mg) mixed ferrites, J alloys compds 526 (2012) 91–97.
[34] I. Chihi, M. Baazaoui, N. Hamdaoui, J.M. Greneche, M. Oumezzine, Kh Farah, Sol–gel synthesis and characterization of magnesium ferrites by XRD, TEM, EPR, Mossbauer, and impedance spectroscopy, J Mater Sci: Mater Electro. 32 (2021) 16634–16647.
[35] K.A. Mohammed, A.D. Al-Rawas, A.M. Gismelseed, A. Sellai, H.M. Widatallah, A. Yousif, M.E. Elzain, M. Shongwe, Infrared and structural studies of Mg1–xZnxFe2O4 ferrites, Physica B: Conden Mat. 407 (4) (2012) 795–804.
[36] B. Babić-Stojić, V. Jokanović, D. Milivojević, Z. Jagličić, D. Makovec, N. Jović, M. Marinović-Cincović, Magnetic and structural studies of CoFe2O4 nanoparticles suspended in an organic liquid, J Nanomate (2013) 9, 741036.
[37] W.A.A. Bayoumy, Synthesis and characterization of nano-crystalline Zn-substituted Mg–Ni–Fe–Cr ferrites via surfactant-assisted route, J Mol Struc 1056 (2014) 285–291.
[38] S. Kanagesan, M. Hashim, S. Tamilselvan, N.B. Alitheen, I. Ismail, G. Bahmanrokh, Cytotoxic effect of nanocrystalline MgFe2O4 particles for cancer cure, J Nanomaterials 2013 (2013) 8, 865024.
[39] T. Arun, K. Prabakaran, R. Udayabhaskar, R.V. Mangalaraja, an A. Akbari-Fakhrabadi, Carbon decorated octahedral shaped Fe3O4 and α-Fe2O3 magnetic hybrid nanomaterials for next generation supercapacitor applications, Appl. Surf. Sci. 485 (2019) 147–157.
[40] T. Arun, Suresh K. Verma, Pritam Kumar Panda, R.J. Joseyphus, E. Jhae, Ali Akbari- Fakhrabadi, P. Sengupta, D.K. Ray, V.S. Benitha, K. Jeyasubramanyan, P. V. Satyam, Facile synthesized novel hybrid graphene oxide/cobalt ferrite magnetic nanoparticles based surface coating material inhibit bacterial secretion pathway for antibacterial effect, Mater Sci Engg: C 104 (2019) 109932.
[41] S. Raghuvanshi, M. Satalkar, P. Tapkir, N.Ghodke S.N. Kane, On the structural and magnetic study of Mg1-xZnxFe2O4, J Phys: Conf Ser 534 (2014) 012031.
[42] E. Suharyadi, E.A. Setiadi, N. Shabrina, T. Kato, S. Iwata, Magnetic properties and microstructures of polyethylene glycol (PEG)-coated cobalt ferrite (CoFe2O4) nanoparticles synthesized by coprecipitation method, Advan Mat Res 896 (2014) 126–133.
[43] A. Manohar, C. Krishnamoorthi, C. Pavithra, N. Thota, Magnetic hyperthermia and photocatalytic properties of MnFe2O4 nanoparticles synthesized by solvothermal reflux method, J Supercon Nov Magne 34 (2021) 251–259.
[44] Y. Jinlin, X. Shuo, Z. Pengyan, M. Shaojian, Comparative study on properties of zinc ferrite and its purified products, J Phys: Conf Ser 2044 (2021) 012068.
[45] T. Arun, T. Kavin kumar, R. Udayabhaskar, Mauricio J. Morel, G. Rajesh, R.V. Mangalaraja, Ali Akbari-Fakhrabadi, Size dependent magnetic and capacitive performance of MnFe2O4 magnetic nanoparticles, Mater. Lett. 276 (2020) 128240.

[46] T. Arun, T. Kavinkumar, R. Udayabhaskar, R. Kiruthiga, Mauricio J. Morel, R. aepuru, N. Dineshbabu, K. Ravichandran, Ali Akbari-Fakhrabadi, R. V. Mangalaraja, NiFe2O4 nanospheres with size-tunable magnetic and electrochemical properties for superior supercapacitor electrode performance, Electrochim. Acta 399 (2021) 139346.
[47] I. Obaidat, M. Bashar Issa, Y. Haik, Magnetic properties of magnetic nanoparticles for efficient hyperthermia, Nanomate 5 (1) (2015) 63–89.
[48] M. Qin, Q. Shuai, G. Wu, B. Zheng, Z. Wang, H. Wu, Zinc ferrite composite material with controllable morphology and its applications, Mater Sci Enggg: B 224 (2017) 125–138.
[49] K. Mukherjee, S.B. Majumder, Synthesis process induced improvement on the gas sensing characteristics of nano-crystalline magnesium zinc ferrite particles, Sensor. Actuator. B Chem. 162 (1) (2012) 229–236.
[50] C. Choodamani, B. Rudraswamy, G.T. Chandrappa, Structural, electrical, and magnetic properties of Zn substituted magnesium ferrite, Ceram Interna 42 (9) (2016) 10565–10571.
[51] H.M. El-Sayed, I.A. Ali, A. Azzam, A.A. Sattar, Influence of the magnetic dead layer thickness of Mg-Zn ferrites nanoparticle on their magnetic properties, J Magne Magne Mat 424 (2017) 226–232.
[52] S. El Shabrawy, C. Bocker, D. Tzankov, M. Georgieva, R. Harizanova, C. Rüssel, The effect of zinc substitution on the magnetism of magnesium ferrite nanostructures crystallized from borate glasses, Ceram Internat 43 (4) (2017) 3804–3810.
[53] A.T. Apostolov, I.N. Apostolova, J.M. Wesselinowa, MO Fe2O3 nanoparticles for self-controlled magnetic hyperthermia, J. Appl. Phys. 109 (8) (2011).
[54] M. Mylarappa, V. Venkata Lakshmi, S. Kantharaju, Recycling and Reusing of Li2CO3 and Co(OH)2 from Waste Lithium ion batteries for energy storage and thermal studies, J Waste Manag Disposal 2 (2019) 301.
[55] S.J. Uke, Satish P. Mardikar, Devidas R. Bambole, Yogesh Kumar, G.N. Chaudhari, Sol-gel citrate synthesized Zn doped MgFe2O4 nanocrystals: a promising supercapacitor electrode material, Mate Sci Energy Tech 3 (2020) 446–455.